

Submitted: July 5, 2025

Revised: September 1, 2025

Accepted: November 12, 2025

Dynamic fracture of concretes with basalt and limestone aggregate at different temperatures

N.S. Selyutina ^{1,2}✉ , D.D. Khairtadinova ^{1,3} 

¹ St. Petersburg State University, St. Petersburg, Russia

² Institute for Problems in Mechanical Engineering of the Russian Academy of Science, St. Petersburg, Russia

³ St. Petersburg State University of Aerospace Instrumentation, St. Petersburg, Russia

✉ nina.selutina@gmail.com

ABSTRACT

The dynamic strength of concrete subjected to variable thermal and velocity conditions is examined, predicated on the incubation time criterion and the thermal fluctuation theory of strength. A salient feature of this criterion is the invariant characteristic time, serving as a quantification of the loading rate. Model validation is accomplished through a comparative analysis of predicted outcomes against empirical data obtained from concrete specimens incorporating basalt, gravel, and limestone aggregates. It is shown that the characteristic relaxation time of concretes increases within the temperature interval of 20 to 800 °C and decreases at temperatures above ~ 800 °C. The temperature dependence of the characteristic relaxation time for concrete with basalt, limestone and gravel aggregate, determining the intensity of the relaxation process, is predicted based on proposed model.

KEYWORDS

dynamic strength • characteristic time • temperature • strain rate • activation energy

Funding. *The study was supported by the Russian Science Foundation (RSF grant 22-11-00091_P).*

Citation: Selyutina NS, Khairtadinova DD. Dynamic fracture of concretes with basalt and limestone aggregate at different temperatures. *Materials Physics and Mechanics*. 2025;53(5): xx–xx.
http://dx.doi.org/10.18149/MPM.5352025_x

Introduction

Temperature and strain rate are key parameters affecting the quasi-static and dynamic strength of concrete. With an increase in the rate of deformation and a fixed temperature, a positive velocity sensitivity of the material is observed, i.e. the dynamic strength increases with the rate of deformation and exceeds the value of static strength. Furthermore, for certain types of concrete [1,2], the commonly held view that both static and dynamic strength decrease with rising temperature above room temperature [3] does not consistently hold across all temperature ranges. In such cases, the quasi-static and dynamic strength of concrete [1,2] above room temperature initially decreases at 200 °C, increases at 400 °C and then declines again at 600 and 800 °C. However, even at these higher temperatures, the strength remains greater than at 200 °C, relative to the values measured at room temperature. The rate of increase of dynamic strength with strain rate with increasing temperature above room temperature may decrease or increase depending on the chemical reactions occurring at a given temperature and different microstructure depending on temperature, as shown in Table 1.

Table 1. Reasons for increase (+) or decrease (-) of static strength of concrete at different temperatures

C-S-H= CaSO ₄ +H ₂ O		-
gel decomposition C-S-H		
20–400 °C	Evaporation of free and capillary water inside concrete.	-
~ 400 °C	C ₃ S (C ₂ S) + H ₂ O → C-S-H-gel+ Ca(OH) ₂	+
	The process of dehydration [4–6] and shrinkage of the C-S-H gel, which strengthens the bond between the aggregate and the cement paste and partially compensates for the loss of strength caused by their difference in deformation.	
400–600 °C	Ca(OH) ₂ →CaO+H ₂ O	-
	Increase in the difference in deformation between the aggregate and concrete paste and decomposition Ca(OH) ₂ .	
< 600 °C	CaCO ₃ →CaO+CO ₂	-
	CaCO ₃ begins to decompose and the aggregate becomes loose.	

At constant temperature during high-speed deformation [7–9], the water content in the samples influences the strength of concrete. Concrete with 0 % water saturation exhibits higher strength under static loads, and water-saturated concrete demonstrates greater strength under dynamic loads. Under static conditions, the phenomenon can be attributed to hydrostatic pressure in water-saturated concrete samples. Conversely, under dynamic conditions, the influence of hydrostatic pressure on concrete strength increases, which leads to a slowdown in the incubation processes during micro-cracking.

The application of thermal fluctuation theory of strength is often used to predict the strength of concrete and other composite materials [10–14]. Although concrete appears robust, temperature fluctuations during service can significantly reduce its lifespan [15]. Thermal stresses caused by temperature variations must always be considered during the design phase of concrete components. Furthermore, the incorporation of alternative materials to enhance sustainability—such as recycled concrete, slag, and plastic aggregates—inevitably affects concrete’s thermal response [16–19]. Key observations include:

1. Recycled concrete aggregates exposed to cyclic thermal loading develop microcracks in the interfacial transition zones, reducing strength [20,21].
2. Slag aggregates, due to their high density, improve thermal resistance, minimizing strength loss at elevated temperatures [22].
3. Plastic aggregates lead to significant strength loss under high temperatures as the plastic particles melt [23,24].

In this paper, a method is proposed for predicting the increase in both static and dynamic strength of concrete with rising temperature, based on the incubation time criterion [7,25,26], while incorporating the thermofluctuation mechanism of fracture [12–14,27–29]. By introducing the concept of incubation time and applying the standard equations of thermofluctuation strength theory, the model enables estimation of a material’s dynamic strength across a wide range of deformation rates and temperatures. The proposed model demonstrates good predictive capability for the strength of concrete containing limestone and basalt aggregates under varying thermal and speed conditions. It is shown that the characteristic relaxation time decreases with increasing temperature up to approximately 1000 K, after which it begins to increase – an anomalous behavior for this parameter.

Incubation time criterion

The instability of strength characteristics in brittle materials under high-speed deformation has been observed in dynamic experiments involving rocks and concrete [1,2,30]. Predicting the distinctive strain rate dependence of material strength across a wide range of strain rates remains one of the central challenges in fracture dynamics. In this paper, a structural-temporal approach previously proposed in studies [7,25,26] is employed to calculate material strength at varying strain rates. Dynamic strength σ_d is defined as the maximum value of the ultimate stress achieved in a sample when it is loaded until fracture. Within the framework of the structural-temporal approach, the fracture condition is expressed as follows:

$$\frac{1}{\tau} \int_{t-\tau}^t \left(\frac{\sigma(t')}{\sigma_c} \right)^\alpha dt' \leq 1, \quad (1)$$

where τ is the incubation time of fracture, $\sigma(t)$ is the time dependence of the stresses in the sample (at the place of fracture), σ_c is the static compressive strength, α is the parameter characterizing the sensitivity of the material to the level of force field intensity that causes compression fracture. Within the framework of the structural-temporal approach, when determining the ultimate strength σ_{ul} , condition (1) is written for each of the loads. In this case, the set of material characteristics α , τ , σ_c differs for the cases of tension and compression. In this work, the strain rate dependence of the compressive strength of concrete is considered. The fracture time t_* is determined from the condition in which the inequality (1) transforms into equality. The incubation time is the characteristic time of relaxation. In the case of fracture, the physical nature of the incubation time is associated with the relaxation processes of micro-cracking before macro-fracture.

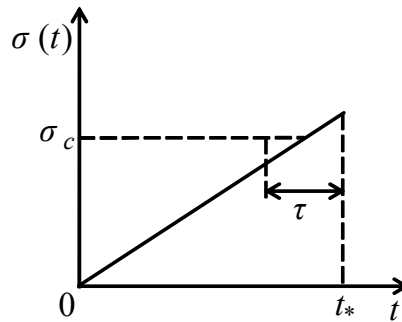


Fig. 1. Temporal dependence of stress for slow linear loading

Fracture criterion (1) implies the existence of an incubation period, preceding a macroscopic failure of the material. In this context, an incubation process is an essential component of the overall fracture process and occurs under both quasi-static and fast impact loads. The presence of this fracture incubation period gives rise to specific phenomena under dynamic loading, most notably the well-established strain-rate dependence of material strength. As one of the simplest interpretations of the fracture incubation time, let us consider an example of fracture caused by a slow ($t_* \gg \tau$) linearly growing tensile stress $\sigma(t) = \dot{\sigma} t H(t)$, where $\dot{\sigma} = \text{const}$ and $H(t)$ is the Heaviside step function. Substituting linear expression for $\sigma(t)$ into (1), we can calculate the time to

fracture $t_* = \sigma_c / \dot{\sigma} + 0.5 \tau$ and a value of the critical stress at the moment of fracture $\sigma_{ul} = \sigma(t_*) = \sigma_c + 0.5 \dot{\sigma} \tau$, where σ_c is the tabulated value of the material static strength. In the case of very slow stress growth $(\dot{\sigma} \tau) / \sigma_c \ll 1$, the ultimate stress does not differ much from the static strength $\sigma_{ul} \approx \sigma_c$. The obtained expressions show that according to Eq. (1) the material remains intact at the moment when the static strength limit is achieved $t_c = \sigma_c / \dot{\sigma}$. It is crucial that before the onset of the macroscopic rupture of the material, preparatory processes having a characteristic temporal period τ evolve in the material structure (Fig. 1).

The main advantage of using the structural-temporal approach is the introduction of the incubation time parameter, which is invariant with respect to the loading history $\sigma(t)$. According to the notion of the incubation time, two concrete specimens with different fibre volume fractions have different incubation time values. The incubation time is determined by approximation methods based on an experimental set of strength and strain rate values. The least squares method is used in this study. The loading of concrete samples in both static and dynamic experiments, as shown in the previous studies [7,25,26], is carried out according to the linear function of deformation in time.

The time dependence of the stresses in the sample has the following form:

$$\sigma(t) = E \dot{\epsilon} t H(t), \quad (2)$$

where E is Young's modulus, $\dot{\epsilon}$ is the strain rate, and $H(t)$ is the Heaviside function. It is noted that wave processes are neglected when measuring the dynamic strength in experiments [1–3] on a split Hopkinson pressure bar, where long-term load pulses are set. Therefore, when assessing strength in a wide range of strain rates based on the structural-temporal approach (1), wave effects are also neglected.

Let us recall that, according to the given definition of strength above, for the case of linear loading, the strength is defined as $\sigma_{ul} = \sigma(t_*) = E \dot{\epsilon} t_*$. Substituting Eq. (2) into the equality condition (1), the dependence of the fracture time on the strain rate $t^*(\dot{\epsilon})$ is determined:

$$t_*(\dot{\epsilon}) = \begin{cases} \left((\alpha + 1) \left(\frac{\sigma_c}{E \dot{\epsilon}} \right)^\alpha \tau \right)^{\frac{1}{\alpha+1}}, & \dot{\epsilon} \geq \sqrt[\alpha]{\alpha + 1} \frac{\sigma_c}{E \tau} \quad (t_* \leq \tau), \\ \frac{\sigma_{ul}^{sol}}{(E \dot{\epsilon})^{\alpha+1}}, & \dot{\epsilon} < \sqrt[\alpha]{\alpha + 1} \frac{\sigma_c}{E \tau} \quad (t_* > \tau), \end{cases} \quad (3)$$

where σ_{ul}^{sol} is the solution to the following equation with respect to σ_{ul} :

$$(\sigma_{ul})^{\alpha+1} - (\sigma_{ul} - E \dot{\epsilon} \tau)^{\alpha+1} = (\alpha + 1) E \dot{\epsilon} \tau \sigma_c^\alpha. \quad (4)$$

Then, by substituting the obtained dependence $t_*(\dot{\epsilon})$ (Eq. (3)) into σ_{ul} , the dependence of the ultimate strength on the strain rate has the following form:

$$\sigma_{ul}(\dot{\epsilon}) = \begin{cases} \left((\alpha + 1) E \dot{\epsilon} \tau \sigma_c^\alpha \right)^{\frac{1}{\alpha+1}}, & \dot{\epsilon} \geq \sqrt[\alpha]{\alpha + 1} \frac{\sigma_c}{E \tau} \quad (t_* \leq \tau), \\ \sigma_{ul}^{sol}(\dot{\epsilon}), & \dot{\epsilon} < \sqrt[\alpha]{\alpha + 1} \frac{\sigma_c}{E \tau} \quad (t_* > \tau). \end{cases} \quad (5)$$

In the case of $\alpha = 1$, Eq. (5) is written explicitly:

$$\sigma_{ul}(\dot{\epsilon}) = \begin{cases} \sqrt{2 E \dot{\epsilon} \tau \sigma_c}, & \dot{\epsilon} \geq \frac{2 \sigma_c}{E \tau} \quad (t_* \leq \tau), \\ \sigma_c + \frac{1}{2} E \dot{\epsilon} \tau, & \dot{\epsilon} < \frac{2 \sigma_c}{E \tau} \quad (t_* > \tau). \end{cases} \quad (6)$$

Thus, Eq. (6) provides a simple description of the ultimate stress across a wide range of strain rates. To estimate the incubation time τ and the amplitude parameter α , the least

squares method is used on a set of experimental data referring to critical stresses and corresponding strain rates. In [7], the process of fracture within the framework of the structural-temporal approach, written at $\alpha = 1$, is considered at various scale levels, and the characteristic of τ is determined at a given scale level. Establishing a set of material parameters σ_c , E , τ makes it possible to construct a non-linear relationship.

Hybrid model

In this section, we define the temperature dependencies for the characteristic relaxation time $\tau(T)$ and introduce them on the basis of the thermofluctuation theory of strength [27,31,32]. In this case, the intensity of the relaxation process is usually considered as a process with an exponential dependence on temperature [27]. The canonical form of the Zhurkov formula has the form (7) for estimating the temperature dependence of the intensity of relaxation processes:

$$\tau(T) = \tau_a \exp\left(\frac{U_0 - \delta\sigma}{kT}\right), \quad (7)$$

where $\tau(T)$ is the effective time to reach a state close to equilibrium (such a movement of the system towards equilibrium is called relaxation) [27], T is temperature, τ_a is the period of oscillation of atoms in a solid ($\tau_a = 10^{-12} \dots 10^{-13}$ s), U_0 is the initial activation energy in the unstressed state of the body (the activation energy of interatomic bonds), δ is the structural coefficient that characterizes the velocity of decrease in activation energy with increasing stress under fracture, $k = 8.314$ J/(K·mol) is the Boltzmann's universal gas constant. The value of the barrier $U(T)$ under the assumptions presented in the work [33] is determined from the measured dependence of $\ln \tau_e(1/T)$:

$$U(T) = kT \ln\left(\frac{\tau_e}{\tau_a}\right), \quad (8)$$

where τ_e is the effective time to reach a state close to equilibrium (such movement of the system towards equilibrium is the relaxation) [27]. Equation (8) showed good agreement with experimental data in the papers [14,34,35] for concrete with sand aggregate in various temperature ranges from -40 to +60 °C [14]; from -5 to -25 °C [34]; from -40 to 0 °C [35].

Based on studies on the long-term strength of concrete in the temperature range from -40 to +60 °C in work [14], it was established: (1) the activation energy of fracture is independent of applied stress and temperature and is equal to 162.8 kJ/mol; (2) the pre-exponential constant, which characterizes the average time between successive thermal oscillations, depends on both stress and temperature; (3) the higher the temperature, the less the effect of stress. In the paper [14], it was proposed to use Zhurkov's formula Eq. (7) in the following generalized form:

$$\tau(T) = \tau_a \sigma(T) \exp\left(\frac{U_0}{kT}\right). \quad (9)$$

In the work [36,37], Zhurkov's formula (Eqs. (7) and (9)) and the structural-time approach [29] were applied to determine the strength dependencies during spall fracture:

$$\tau(T) = \tau_a \exp\left(\frac{U_0 - \delta\sigma}{kT}\right) - \frac{t_i}{2}, \quad (10)$$

where t_i is the pulse duration. In this paper, the intensity of the relaxation process is proposed to be written as decreasing and increasing exponential dependencies:

$$\tau(T) = \tau_a \exp\left(\frac{U_0}{kT}\right) + \tau_1 \exp\left(\frac{T_m}{T - T_m}\right), \quad (11)$$

where T_m is the melting temperature, τ_1 is material's constant.

Velocity dependencies of the strength of concretes with basalt and limestone aggregate

Within the framework of the incubation time criterion, theoretical dependencies of strength on the strain rate were developed for concretes produced with limestone aggregate (concrete L), gravel aggregate (concrete G) and with basalt aggregate (concretes B1 and B2), based on experimental data [1–3]. Table 2 shows Mix proportions of concrete [1–3]. Dynamic and static experiments on compressive strength in [1,3] were carried out at different fixed temperatures: 20, 400, 650, 800, and 950 °C for concrete with basalt aggregate [3] and 20, 200, 400, 600, and 800 °C for concretes with limestone aggregate [1] and gravel aggregate [2]. For each temperature illustrated in Fig. 2, two theoretical strength dependencies on strain rate were plotted, indicated by solid lines: one curve intersected the minimum experimental point ($\dot{\epsilon}, \sigma_{ul}$), while the other aligned with the maximum experimental point ($\dot{\epsilon}, \sigma_{ul}$). As a result, the range of experimental values ($\dot{\epsilon}, \sigma_{ul}$) was between these two theoretical dependencies. The values of Young's modulus and static strength for each temperature are set according to experimental data [1,3] from stress-strain relationships and take a fixed value for each temperature. The two theoretical dependencies of strength on the strain rate for concretes B1, B2 and L differed only in the fracture characteristic time, thereby setting the characteristic time interval for each temperature: from 80.8 to 135.4 μs at 20 °C; from 42.35 to 95 μs at 400 °C; from 19.4 to 64.1 μs at 650 °C; from 17.4 to 47.67 μs at 800 °C; from 88.6 to 227.3 μs at 950 °C for concretes B1 and B2; from 39.9 to 97.1 μs at 20 °C, from 60.1 to 82 μs at 200 °C, from 78.6 to 157.86 μs at 400 °C, from 122.5 to 181.46 μs at 600 °C, from 247.2 to 350.8 μs at 800 °C for concrete L and from 49.14 to 89.71 μs at 20 °C, from 39.92 to 67.28 μs at 200 °C, from 60.92 to 94.88 μs at 400 °C, from 121.54 to 128.14 μs at 600 °C, from 86.88 to 194.43 μs at 800 °C for concrete G. For the entire set of experimental values ($\dot{\epsilon}, \sigma_{ul}$), the parameter of the average characteristic time is also determined for both concretes:

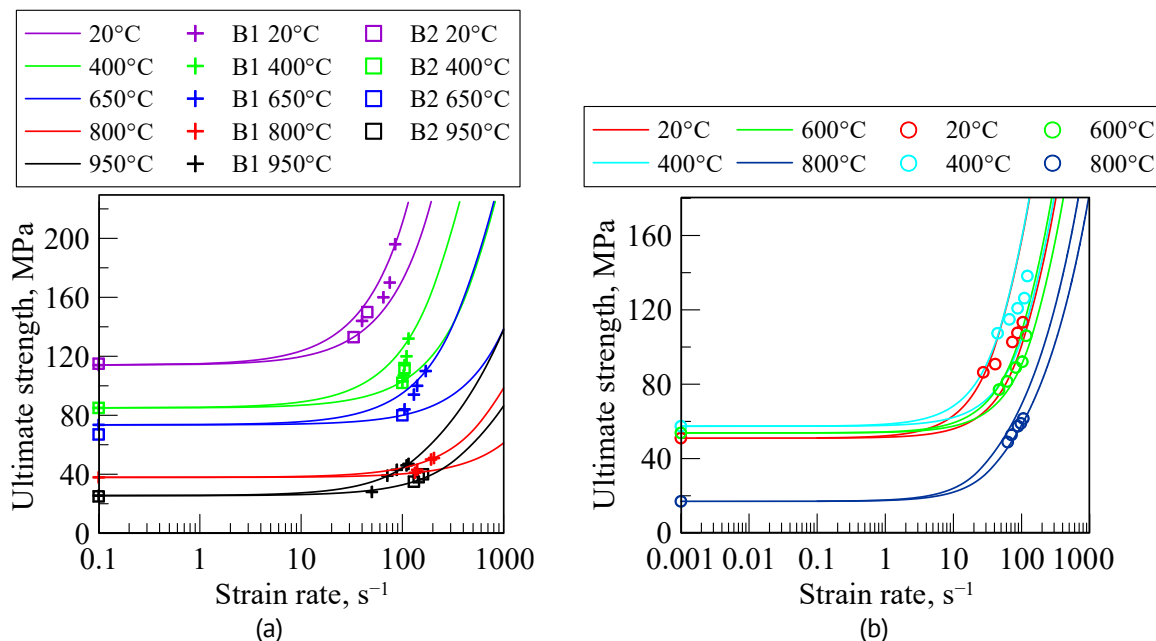


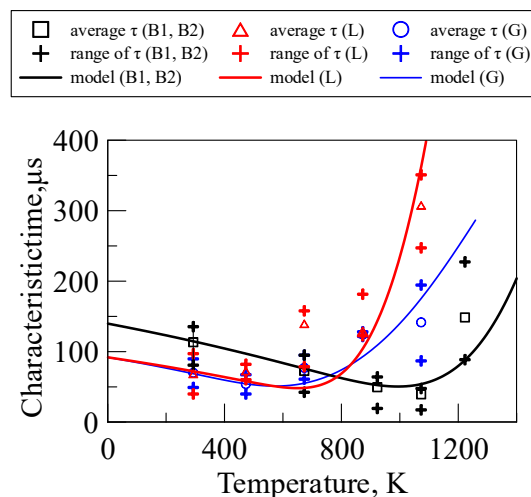
Fig. 2. The range of theoretical speed dependencies of concrete strength at different temperatures, plotted on experimental data by tests of concrete (a) B1 and B2 [3]; (b) L [1]

Table 2. Mix proportions of concrete [1,3]

Designation for this work	Concrete B1	Concrete B2	Concrete L	Concrete G
Reference	[3] (concrete C)	[3] (concrete B)	[1]	[2]
Water, kg/m ³	166	179	180	180
Cement, kg/m ³	442	391	371	600
Fly ash, kg/m ³	78	69	99	-
Sand, kg/m ³	689	689	672	668
Admixture, kg/m ³	5.3	3.5	5	9
Aggregate, kg/m	1125	1172	1008	1002
Material of aggregate	Basalt	Basalt	Limestone	Gravel

113.4 μs at 20 $^{\circ}\text{C}$; 72.62 μs at 400 $^{\circ}\text{C}$; 49.5 μs at 650 $^{\circ}\text{C}$; 39.4 μs at 800 $^{\circ}\text{C}$; 148.5 μs at 950 $^{\circ}\text{C}$ for concretes B1 and B2; at 68.5 μs 20 $^{\circ}\text{C}$, 72.65 μs at 200 $^{\circ}\text{C}$, 139.65 μs at 400 $^{\circ}\text{C}$, 129.65 μs at 600 $^{\circ}\text{C}$, 307.55 μs at 800 $^{\circ}\text{C}$ for concrete L and 69.9 μs 20 $^{\circ}\text{C}$, 54.07 μs at 200 $^{\circ}\text{C}$, 77 μs at 400 $^{\circ}\text{C}$, 124.37 μs at 600 $^{\circ}\text{C}$, 141.59 μs at 800 $^{\circ}\text{C}$ for concrete G.

We develop the temperature dependence of the incubation time using a hybrid model of Eq. (11) for the derived range of characteristic times, on the basis of which the theoretical dependencies of strength on the strain rate were calculated in Fig. 2. Parameters for the theoretical temperature dependencies of characteristic time: (black curve, B1 and B2) $\tau_1=380 \mu\text{s}$, $U_0=2374 \text{ kJ/mol}$, $T_m=1773 \text{ K}$; $\tau_1=250 \mu\text{s}$ $U_0=195.3 \text{ kJ/mol}$, $T_m=1500 \text{ K}$ (red curve, concrete L) and $\tau_1=250 \mu\text{s}$ $U_0=30 \text{ kJ/mol}$, $T_m=1300 \text{ K}$. The obtained values of the activation energy for concrete are close to the value $U_0=162.8 \text{ kJ/mol}$ obtained in [18] for concrete. As shown in Fig. 3, the incubation time for concretes with limestone and gravel aggregate increases with temperature, whereas for concrete with basalt aggregate, it initially decreases up to 800 $^{\circ}\text{C}$ and then increases. Figure 3 shows that the incubation time for concretes with limestone and gravel aggregate increases with temperature, whereas for concrete with basalt aggregate, it initially decreases up to 800 $^{\circ}\text{C}$, after which it begins to increase.

**Fig. 3.** Temperature dependencies of the characteristic time of concrete B1, B2, L and G





At high temperatures, the influence of inertial forces on the strength of the concrete is dominant, since the concrete structure has more cracks and an increased water content. The latter effect, combined with inertial forces, makes it possible to increase the

characteristic and dynamic strength at the same time. The resulting effect is considered anomalous because the typical dependence at high temperatures is a decreasing function of relaxation time.

Conclusions

The rate dependences of concrete strength at different temperatures, plotted on experimental data by tests of concrete with basalt and limestone aggregate, were predicted based on the incubation time criterion. The proposed model accurately predicts the strength of concrete with limestone, gravel and basalt aggregates under varying temperature and loading rate conditions. Based on the incubation time criterion and the theoretical construct of thermofluctuation strength, two discrete temperature-dependent characteristic time functions were ascertained: one pertinent to concretes incorporating limestone and gravel aggregate and another specific to concrete with basalt aggregate. It is evinced by the inquiry that the influence of aggregate composition is exerted on both the velocity of dynamic strength enhancement and the characteristic relaxation time.

CRedit authorship contribution statement

Nina S. Selyutina  : writing – review & editing, writing – original draft, the main idea, state of the problem, conceptualization, analysis of the result, hybrid model, supervision; **Diana D. Khairtadinova**  : writing – original draft, analysis of the result, investigation.

Conflict of interest

The authors declare that they have no conflict of interest.

References

1. Su H, Xu J, Ren W. Experimental study on the dynamic compressive mechanical properties of concrete at elevated temperature. *Materials & Design*. 2014;56: 579–588.
2. Li L, Zhang R, Jin L, Du X, Wu J, Duan W. Experimental study on dynamic compressive behavior of steel fiber reinforced concrete at elevated temperatures. *Construction and Building Materials*. 2019;210: 673–684.
3. Chen L, Fang Q, Jiang X, Ruan Z, Hong J. Combined effects of high temperature and high strain rate on normal weight concrete. *International Journal of Impact Engineering*. 2015;86: 40–56.
4. Ma Q, Guo R, Zhao Z, Lin Z, He K. Mechanical properties of concrete at high temperature - A review. *Construction and Building Materials*. 2015;93: 371–383.
5. Arioiz O. Effects of elevated temperatures on properties of concrete. *Fire Safety Journal*. 2007;42(8): 516–522.
6. Pan Z, Sanjayan JG. Stress–strain behaviour and abrupt loss of stiffness of geopolymers at elevated temperatures. *Cement and Concrete Composites*. 2010;32(9): 657–664.
7. Selyutina NS, Petrov YuV. Dynamic strength and fracture of brittle materials under shock-wave loading. *Engineering Fracture Mechanics*. 2020;225: 106265.
8. Selyutina N, Smirnov I. Dynamic deformation and fracture of structured materials under high-rate loading. *Mechanics of Materials*. 2023;179: 104613.
9. Selyutina NS, Khairtadinova DD. Dynamic Fracture of Fibre-Reinforced Concrete Depending on the Shape and Material of the Reinforcing Fibre. *Journal of Dynamic Behavior of Materials*. 2025;11: 34–44.
10. Rudskoy AI, Bashkarev AY, Bessonova VY. Application of the thermofluctuation theory of strength to calculate the durability of adhesive joints on the example of granite-bitumen composites. In: *Systems*

- Analysis in design and management: collection of scientific papers of the XXVI International scientific and practical conference, October 13-14, 2022.* 2022. p.507–520. (In Russian)
11. Revilla-Cuesta V, Hurtado-Alonso N, Manso-Morato J, Serrano-López R, Manso JM. Effects of temperature and moisture fluctuations for suitable use of raw-crushed wind-turbine blade in concrete. *Environmental Science and Pollution Research*. 2024;31(25): 37757–37776.
 12. Kartashov EM. Advanced materials for extreme environments: Synthesis and characterization. *Fine Chemical Technologies*. 2021;16(6): 526–540.
 13. Asadi I, Shafiqh P, Hassan ZFBA, Mahyuddin NB, Thermal conductivity of concrete – A review. *Journal of Building Engineering*. 2018;20: 81–93.
 14. Iskakbayev AI, Teltayev BB, Yestayev KZ, Abu BD. Long-term strength of asphalt concrete and its applications. *Construction and Building Materials*. 2020;244: 118325.
 15. Ferronato N, Fuentes Sirpa RC, Guisbert Lizarazu EG, Conti F, Torretta V. Construction and demolition waste recycling in developing cities: management and cost analysis. *Environmental Science and Pollution Research*. 2023;30(9): 24377–24397.
 16. Xu GT, Liu MJ, Xiang Y, Fu B. Valorization of macro fibers recycled from decom-missioned turbine blades as discrete reinforcement in concrete. *Journal of Cleaner Production*. 2022;379: 134550.
 17. Xu J, Xiong W, Guo X, Lai T, Liu Y, Ying W. Properties of using excavated soil waste as fine and coarse aggregates in unfired clay bricks after dry-wet cycles. *Case Studies in Construction Materials*. 2022;17: e01471.
 18. Çeçen F, Aktaş B, Özbayrak A. Decarbonization of the concrete railway sleeper production: bringing the low-dosage pozzolanic cement usage in the sleeper production via novel laminated CFRPU reinforcement technique. *Materials Today Sustainability*. 2023;23: 100455.
 19. Li L, Yu H, Zhou S, Dao V, Chen M, Ji L, Benhelal E. Activation and utilization of tailings as CO₂ mineralization feedstock and supplementary cementitious materials: a critical review. *Materials Today Sustainability*. 2023;24: 100530.
 20. Revilla-Cuesta V, Skaf M, Santamaría A, Espinosa AB, Ortega-López V. Self-compacting concrete with recycled concrete aggregate subjected to alternating-sign temperature variations: thermal strain and damage. *Case Studies in Construction Materials*. 2022;17: e01204.
 21. Munoz Perez SP, Salazar Pretel TM, Villena Zapata LI. Mechanical properties of a soil improved with recycled demolition concrete for the construction of shallow foundations. *Materials Physics and Mechanics*. 2023;51(1): 168–178.
 22. Beaucour AL, Pliya P, Faleschini F, Njinwoua R, Pellegrino C, Noumowé A. Influence of elevated temperature on properties of radiation shielding concrete with electric arc furnace slag as coarse aggregate. *Construction and Building Materials*. 2020;256: 119385.
 23. Tariq KA, Rehman MU, Ghafran R, Kamran I, Haroon M. Physio-mechanical and thermal properties of concrete produced by partial replacement of sand with plastic fines. *Proceedings of the Pakistan Academy of Sciences: A*. 2021;57(3): 61–68.
 24. Erofeev VT, Korotaev SA, Vatin NI. Deformation and Heat-Insulating Characteristics of Light Concrete on Porous Burned Binder Under Heating. *Materials Physics and Mechanics*. 2023;51(1): 33–41.
 25. Petrov YV, Gruzdkov AA, Bratov VA. Structural-temporal theory of fracture as a multiscale process. *Phys Mesomech*. 2012;15: 232–237.
 26. Petrov YV, Smirnov IV, Volkov GA, Abramian AK, Bragov AM, Verichev SN. Dynamic failure of dry and fully saturated limestone samples based on incubation time concept. *Journal of Rock Mechanics and Geotechnical Engineering*. 2017;9(1): 125–134.
 27. Solov'eva YV, Starenchenko SV, Starenchenko VA. Energy of Activation of the Plastic Deformation of Ni₃Ge Single Crystals with Different Orientations of the Axis of Compression. *Bulletin of the Russian Academy of Sciences: Physics*. 2020;84: 1582–1585.
 28. Goldenberg BG, Rakshun YV, Bugaev SV, Meshkov OI, Tsybulya SV. Designing a Technological Station for Synchrotron Radiation on the VEPP-4M. *Bulletin of the Russian Academy of Sciences: Physics*. 2019;83: 129–133.
 29. Glebovskii PA, Petrov YV. Kinetic interpretation of the structural-time criterion for fracture. *Phys. Solid State*. 2004;46: 1051–1054.
 30. Smirnov I, Konstantinov A. Evaluation of critical stresses for quasi-brittle materials at various loading rates. *Materials Physics and Mechanics*. 2020;44(2): 210–220.
 31. Zhurkov SN. Kinetic Concept of the Strength of Solids. *Int J Fract*. 1965;1: 311–323.

32. Regel VR, Slutsker AI, Tomashevskiy EE. *Kinetic Nature of Solid Body Strength*. Moscow: Nauka; 1974. (In Russian)
33. Slutsker AI, Polikarpov YI, Vasil'eva KV. Determination of the activation energy for complicated relaxation processes. *Physics of the Solid State*. 2002;44: 1604-1610.
34. Gubach LS, Fisher EK. About the use of kinetic theory of solid bodies strength in investigation of asphalt concrete service life in conditions of low temperatures. In: *Efficiency Increase for the Use of Cement and Asphalt Concretes in Siberia. Interuniversity Collection*. 1979. p.3-9. (In Russian)
35. Nickolskiy YuE, Pisklin VM, Shestakov VN. About long-term strength of asphalt concrete within the interval of temperatures from 233 to 273 K. In: *Efficiency Increase for the Use of Cement and Asphalt Concretes in Siberia. Interuniversity Collection*. 1979. p.10–17. (In Russian)
36. Zhurkov SN. Kinetic concept of the strength of solids. *Int J Fract*. 26, 295–307 (1984).
37. Suhir E, Kang SM. Boltzmann–Arrhenius–Zhurkov (BAZ) model in physics-of-materials problems. *Modern Physics Letters B*. 2013;27(13): 1330009.